AUTOPHAGY
2024, VOL. 20, NO. 3, 659–674
https://doi.org/10.1080/15548627.2024.2305063

Taylor & Francis
Taylor & Francis Group

RESEARCH PAPER

ANXA2 (annexin A2) is crucial to ATG7-mediated autophagy, leading to tumor aggressiveness in triple-negative breast cancer cells

Minsoo Koh[a,b*], Hyesol Lim[a*], Hao Jin[a*], Minjoo Kim[a], Yeji Hong[a], Young Keun Hwang[a], Yunjung Woo[a], Eun-Sook Kim[a], Sun Young Kim[c], Kyung Mee Kim[a], Hyun Kyung Lim[a], Joohee Jung[a], Sujin Kang[b], Boyoun Park[b], Han-Byoel Lee[d], Wonshik Han[d,e], Myung-Shik Lee[f], and Aree Moon[a]

[a]Duksung Innovative Drug Center, College of Pharmacy, Duksung Women's University, Seoul, Korea; [b]Department of Systems Biology, College of Life Science and Biotechnology, Yonsei University, Seoul, South Korea; [c]Department of Chemistry, College of Science and Technology, Duksung Women's University, Seoul, Korea; [d]Department of Surgery, Seoul National University College of Medicine, Seoul, Korea; [e]Cancer Research Institute, Seoul National University College of Medicine, Seoul, Korea; [f]Avison Biomedical Research Center, Yonsei University College of Medicine, Seoul, Korea

ABSTRACT

Triple-negative breast cancer (TNBC) is associated with a poor prognosis and metastatic growth. TNBC cells frequently undergo macroautophagy/autophagy, contributing to tumor progression and chemotherapeutic resistance. ANXA2 (annexin A2), a potential therapeutic target for TNBC, has been reported to stimulate autophagy. In this study, we investigated the role of ANXA2 in autophagic processes in TNBC cells. TNBC patients exhibited high levels of ANXA2, which correlated with poor outcomes. ANXA2 increased LC3B-II levels following bafilomycin A_1 treatment and enhanced autophagic flux in TNBC cells. Notably, ANXA2 upregulated the phosphorylation of HSF1 (heat shock transcription factor 1), resulting in the transcriptional activation of *ATG7* (autophagy related 7). The mechanistic target of rapamycin kinase complex 2 (MTORC2) played an important role in ANXA2-mediated *ATG7* transcription by HSF1. MTORC2 did not affect the mRNA level of *ANXA2*, but it was involved in the protein stability of ANXA2. HSPA (heat shock protein family A (Hsp70)) was a potential interacting protein with ANXA2, which may protect ANXA2 from lysosomal proteolysis. ANXA2 knockdown significantly increased sensitivity to doxorubicin, the first-line chemotherapeutic regimen for TNBC treatment, suggesting that the inhibition of autophagy by ANXA2 knockdown may overcome doxorubicin resistance. In a TNBC xenograft mouse model, we demonstrated that ANXA2 knockdown combined with doxorubicin administration significantly inhibited tumor growth compared to doxorubicin treatment alone, offering a promising avenue to enhance the effectiveness of chemotherapy. In summary, our study elucidated the molecular mechanism by which ANXA2 modulates autophagy, suggesting a potential therapeutic approach for TNBC treatment.

Abbreviation: ATG: autophagy related; ChIP: chromatin-immunoprecipitation; HBSS: Hanks' balanced salt solution; HSF1: heat shock transcription factor 1; MTOR: mechanistic target of rapamycin kinase; TNBC: triple-negative breast cancer; TFEB: transcription factor EB; TFE3: transcription factor binding to IGHM enhancer 3

ARTICLE HISTORY
Received 14 April 2023
Revised 27 December 2023
Accepted 29 December 2023

KEYWORDS
Annexin A2; ATG7; autophagy; HSF1; MTOR; triple-negative breast cancer

Introduction

Triple-negative breast cancer (TNBC), which is an estrogen receptor-, progesterone receptor-, and human epidermal growth factor receptor 2-negative subtype, has been associated with poor prognosis and metastatic growth [1]. Although multiple genetic and epigenetic factors have been correlated with uncontrolled progression and metastatic spread of TNBC, there is currently no effective therapeutic remedy against TNBC [2].

Cells undergo the basal level of autophagy to maintain homeostasis, and autophagy is facilitated under stress conditions such as nutrient depletion, resulting in either cell survival or death [3]. The MTOR (mechanistic target of rapamycin kinase) signaling pathway is closely involved in sensing energy, nutrients, and stress, which are relevant to the execution of autophagy, survival and cell growth [4,5]. The role of autophagy in cancer has been controversial: it has been shown to either stimulate or inhibit cancer depending on different circumstances such as tumor stage [6]. A recent study has shown that autophagy promotes primary tumor growth yet suppresses metastatic outgrowth in mammary cancer models, suggesting that the effect of autophagy in breast cancer progression is a double-edged sword [7]. The dissemination of dormant breast cancer cells triggers autophagy, and the inhibition of autophagy significantly decreases the metastatic recurrence of breast cancer cells [8].

Recent studies have shown that autophagy of TNBC contributes to tumor progression and chemotherapeutic resistance [9–12]. Autophagy-related markers such as BECN1, LC3A and LC3B have been reported to be highly expressed

CONTACT Aree Moon armoon@duksung.ac.kr College of Pharmacy, Duksung Women's University, 33, Samyang-ro 144-gil, Dobong-Gu, Seoul 01369, Korea
*These authors contributed equally to this study.
Supplemental data for this article can be accessed online at https://doi.org/10.1080/15548627.2024.2305063

in tumor tissues of TNBC patients [13,14]. A high level of LC3B has also been shown to correlated with a poor outcome in TNBC patients [10]. These studies suggest that the inhibition of autophagy may be an effective anti-cancer strategy against TNBC [9,10,13,14].

ANXA2 is a Ca^{2+}-dependent phospholipid-binding protein [15] that is important for cytoskeletal rearrangement, cell proliferation, and motility [16,17]. ANXA2 has been suggested to be an emerging biomarker and potential therapeutic target for aggressive cancers, including TNBC [18]. Several laboratories including ours have demonstrated that the upregulation of ANXA2 is correlated with invasive breast cancer cell phenotypes in TNBC cells [19–21] and aggressiveness in TNBC patients [22]. ANXA2 has been shown to stimulate autophagy in HeLa cells [23] and dendritic cells [24] with the involvement of ATG9A (autophagy related 9A) and ATG16L1. Starvation-induced ANXA2 is an important modulator of autophagy fluctuation, and its deficiency reduces autophagy [25]. However, there has yet to be a study detailing the involvement of ANXA2 in autophagic mechanisms in breast cancer.

HSF1 (heat shock transcription factor 1) is a master regulator of the heat shock response and controls the expression of heat shock proteins. Additionally, HSF1 has been shown to regulate non-heat shock response genes that support highly malignant human cancers [26,27]. HSF1 is inactive in its monomeric form and is present in both the cytoplasm and nucleus in the resting state [28]. Under stress conditions, HSF1 trimerizes and more readily translocates to the nucleus. In the nucleus, HSF1 is further phosphorylated and fully activated to enhance its transcriptional activity during heat shock [29]. Previous research has shown that treatment with a chemotherapeutic agent increases trimer formation and nuclear translocation of HSF1 [30]. HSF1 has been reported to induce autophagy by directly regulating *ATG7* transcription, which plays an important role in chemoresistance [30].

In an effort to identify an effective target against TNBC and elucidate the underlying molecular mechanisms, our study explored the potential involvement of ANXA2 in autophagy. We demonstrated that ANXA2 upregulated the phosphorylation of HSF1, resulting in the transcriptional activation of *ATG7* and promoting autophagic flux in TNBC cells. Additionally, ANXA2 knockdown, in combination with doxorubicin treatment, increased doxorubicin sensitivity *in vitro* and inhibited tumor growth in a TNBC xenograft model. Collectively, our findings suggest that ANXA2 is an effective autophagy modulator and a promising therapeutic candidate for targeting TNBC.

Results

ANXA2 level is elevated in TNBC subtype and its expression correlates with poor outcomes of TNBC patients

To explore the association of ANXA2 with TNBC, the Gene Expression Omnibus (GEO) database was used to define the expression level of ANXA2 in breast cancer cell lines and tissues from breast cancer patients (GSE36693). The ANXA2 level was found to be significantly higher in TNBC than non-TNBC subtype in both cell lines and patient tissues (Figure 1A). To examine the correlation between ANXA2 expression and survival in TNBC, the Kaplan-Meier survival curves (with $n = 107$) were obtained based on the GEO data of TNBC patients (GSE58812). The Kaplan-Meier survival curves showed that the high expression of ANXA2 was inversely correlated with overall survival (Figure 1B, left) and metastasis-free survival (Figure 1B, right) of TNBC patients with $p = 0.012$ and $p = 0.014$, respectively. The results indicated that high expression of ANXA2 was associated with a poor outcome for TNBC patients.

ANXA2 is a critical factor in the autophagic flux in TNBC cells

Because autophagy has previously been shown to be involved in TNBC progression [9,10,13,14], it is important to investigate if ANXA2 regulates autophagy of TNBC cells. Hs578T TNBC cells were subjected to starvation with Hanks' balanced salt solution (HBSS) for up to 6 h. The level of ANXA2 remained unchanged, while the expression of LC3B and SQSTM1/p62 decreased in a time-dependent manner (Fig. S1A). Using immunofluorescence microscopy, we observed that ANXA2 and LC3B partially co-localized in the cell peripheral region under nutrients condition. Upon starvation for 2 h, ANXA2 was repositioned along LC3B in the perinuclear region (Fig. S1B), suggesting that ANXA2 may involve in autophagosome trafficking and the autophagic flux process under starvation conditions, consistent with the previous studies [23,24].

LC3B-II is necessary for phagophore expansion and autophagosome formation during the autophagy process [31,32]. The level of LC3B-II was decreased by stable or transient silencing of ANXA2 in starvation condition (Figure 1C and Fig. S1C). The decreased level of LC3B-II indicated either a decrease in autophagosome formation or an increase in autophagosomal degradation [31,32]. To examine these two possibilities, cells were treated with bafilomycin A_1, which is an inhibitor of autophagosome-lysosome fusion that inhibits autophagosomal degradation, thus leading to the accumulation of LC3B-II. The silencing of ANXA2 significantly reduced the bafilomycin A_1-accumulated LC3B-II (Figure 1C and Fig. S1C). ANXA2 overexpression led to an increase in LC3B-II levels upon bafilomycin A_1 treatment (Figure 1E), suggesting that ANXA2 regulates autophagosome formation in TNBC cells.

To investigate the involvement of ANXA2 in autophagy flux, we utilized the pH-sensitive tandem reporter RFP-GFP-LC3 [31,32]. ANXA2 silencing led to a decrease in the number of RFP^+ GFP^+ LC3 puncta (autophagosomes) and RFP^+ GFP^- LC3 puncta (autolysosomes) during starvation, as shown in Figure 1D. ANXA2 overexpression significantly increased both autophagosomes and autolysosomes (Figure 1F). We also observed that ANXA2 regulated autophagosomes in nutrient-rich conditions (Fig. S1D and S1E). These findings collectively demonstrate the significant role of ANXA2 in inducing autophagic flux.

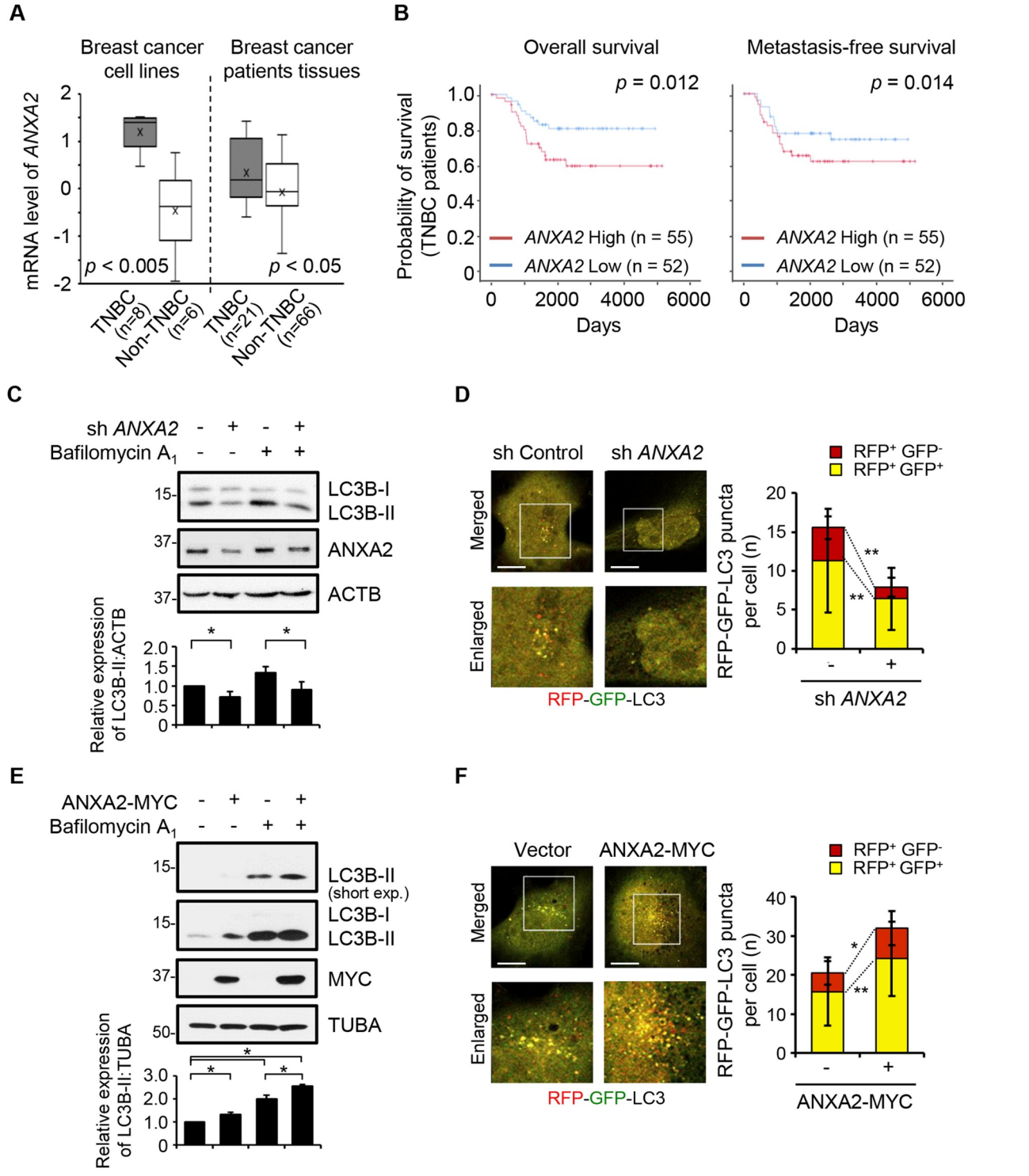

Figure 1. ANXA2 is a critical factor in the autophagic flux in TNBC cells. (A) *ANXA2* mRNA expression in breast cancer cell lines and human breast cancer tissues from GEO dataset (GSE36693). (B) The kaplan-meier survival curves of ANXA2 for overall survival (left) and metastasis-free survival (right) in TNBC patients based on GEO dataset (GSE58812). Patients were divided into groups of low ($n = 52$) and high ($n = 55$) expression based on the median value of *ANXA2* mRNA expression. (C) Hs578T cells were transfected with shRNA targeting *ANXA2* (+) or scrambled shRNA (-) as a control. The cells were starved in HBSS and treated with 200 nM bafilomycin A_1 for 2 h. Immunoblot analysis was conducted. The relative band intensities of LC3B-II were quantified by densitometry and normalized to ACTB. (D) Representative images of LC3 puncta. Hs578T cells expressing shRNA *ANXA2* or scrambled shRNA were transfected with RFP-GFP-LC3 and starved with HBSS for 2 h. LC3 puncta were quantified by the number of RFP^+ GFP^- (red) and RFP^+ GFP^+ (yellow) per cell of 40 independent images. Scale bar of images: 10 μm. (E) Hs578T cells were transfected with plasmid expressing ANXA2-MYC (+) or empty plasmid (-). The cells were starved in HBSS and treated with 200 nM bafilomycin A_1 for 2 h. Immunoblot analysis was conducted. The relative band intensities of LC3B-II were quantified by densitometry and normalized to ACTB. (F) Representative images of LC3 puncta. Hs578T cells expressing ANXA2-MYC or empty vector were transfected with RFP-GFP-LC3 and starved with HBSS for 2 h. LC3 puncta were quantified by the number of RFP^+ GFP^- (red) and RFP^+ GFP^+ (yellow) per cell of 40 independent images. Scale bar of images: 10 μm. Data represent mean ± S.E. (unpaired two-tailed Student's *t*-test). *,** statistically significant at $p < 0.05$ and $p < 0.01$, respectively. All data were representative of the results of three independent experiments.

ANXA2 plays a key role in HSF1-induced transcription of ATG7

ATG7, functioning as a ubiquitin-activating enzyme, plays pivotal roles in the formation of autophagosomes. Recently, it has emerged as associated with human pathologies, including neurodegeneration, cancer, and infection [33]. Given the close association of ATG7 with TNBC, we were prompted to further investigate the interactive roles of ANXA2 and ATG7 [30]. Knockdown of ANXA2 decreased the protein levels of ATG7 in both nutrient-rich and starvation conditions (Figure 2A). The mRNA level of *ATG7* was significantly decreased by silencing ANXA2 (Figure 2B and Fig. S2A). However, the silencing of ATG7 did not affect the expression of ANXA2 (Fig. S2B). ANXA2 promoted the expression of ATG7 protein and mRNA levels (Figure 2C,D), suggesting that ANXA2 may regulate the transcription of *ATG7* in TNBC cells.

HSF1 has been demonstrated to control autophagy through the transcriptional regulation of ATG7 in its phosphorylated form [30]. The phosphorylated form of HSF1 was significantly decreased by silencing ANXA2 (Figure 3A). ANXA2 overexpression led to an increase in phosphorylated (p)-HSF1 expression which was linked to the expression of ATG7 (Figure 3B). To further investigate the localization of p-HSF1, immunofluorescence analysis was conducted. Interestingly, p-HSF1 was predominantly located in the nucleus, and higher fluorescence intensity of p-HSF1 was observed in ANXA2-overexpressing cells compared to the control (Figure 3C). The translocation of TFEB (transcription factor EB) and TFE3 (transcription factor binding to IGHM enhancer 3) into the nucleus increased upon starvation stimulation, but ANXA2 overexpression itself did not seem to affect the translocation of TFEB or TFE3 into the nucleus (Fig. S3A and S3B). Immunofluorescence analysis also revealed that the silencing of HSF1 in the nucleus was associated with a decrease in ATG7 fluorescence intensity (Fig. S4). These data demonstrate that ANXA2 upregulates p-HSF1 and ATG7 expression, leading to enhanced autophagic flux under starvation.

We next examined the role of ANXA2 in binding of HSF1 to the promoter of ATG7 using the chromatin-immunoprecipitation (ChIP) assay. Starvation increased the binding of HSF1 to a promoter region of *ATG7* encompassing

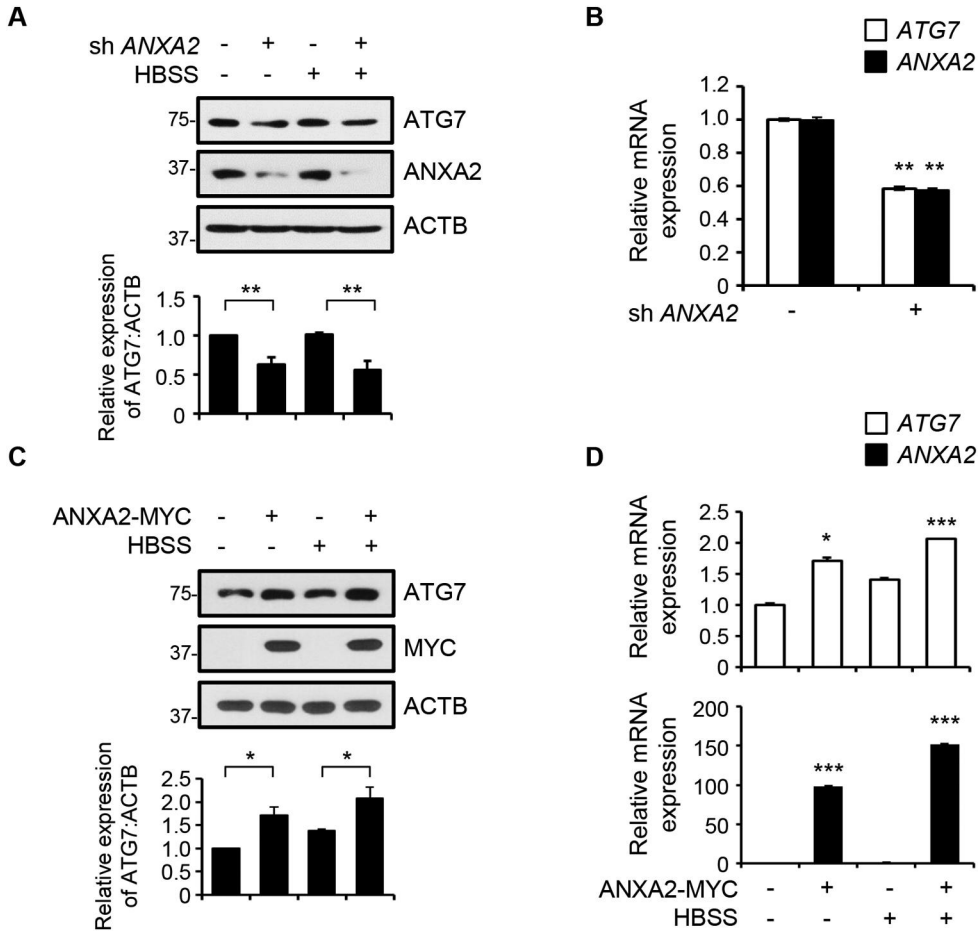

Figure 2. ANXA2 regulates ATG7 transcription. (A and B) Hs578T cells were stably transfected with shRNA targeting *ANXA2* (+) or scrambled shRNA as a control (-). The cells were starved in HBSS for 2 h. The expressions of ATG7 and ANXA2 were detected by immunoblotting (A) and qRT-PCR (B). The relative band intensities of ATG7 were quantified by densitometry and normalized to ACTB in immunoblot analysis. (C and D) Hs578T cells were transfected with ANXA2-MYC vector (+) or empty vector (-) and then the cells were starved in HBSS for 2 h. The expressions of ATG7 and ANXA2 were detected by immunoblotting (C) and qRT-PCR (D). The relative band intensities of ATG7 were quantified by densitometry and normalized to ACTB in immunoblot analysis. Data represent mean ± S.E. (unpaired two-tailed Student's *t*-test). *,**,*** statistically significant at $p < 0.05$, $p < 0.01$, and $p < 0.001$ respectively. All data were representative of the results of three independent experiments.

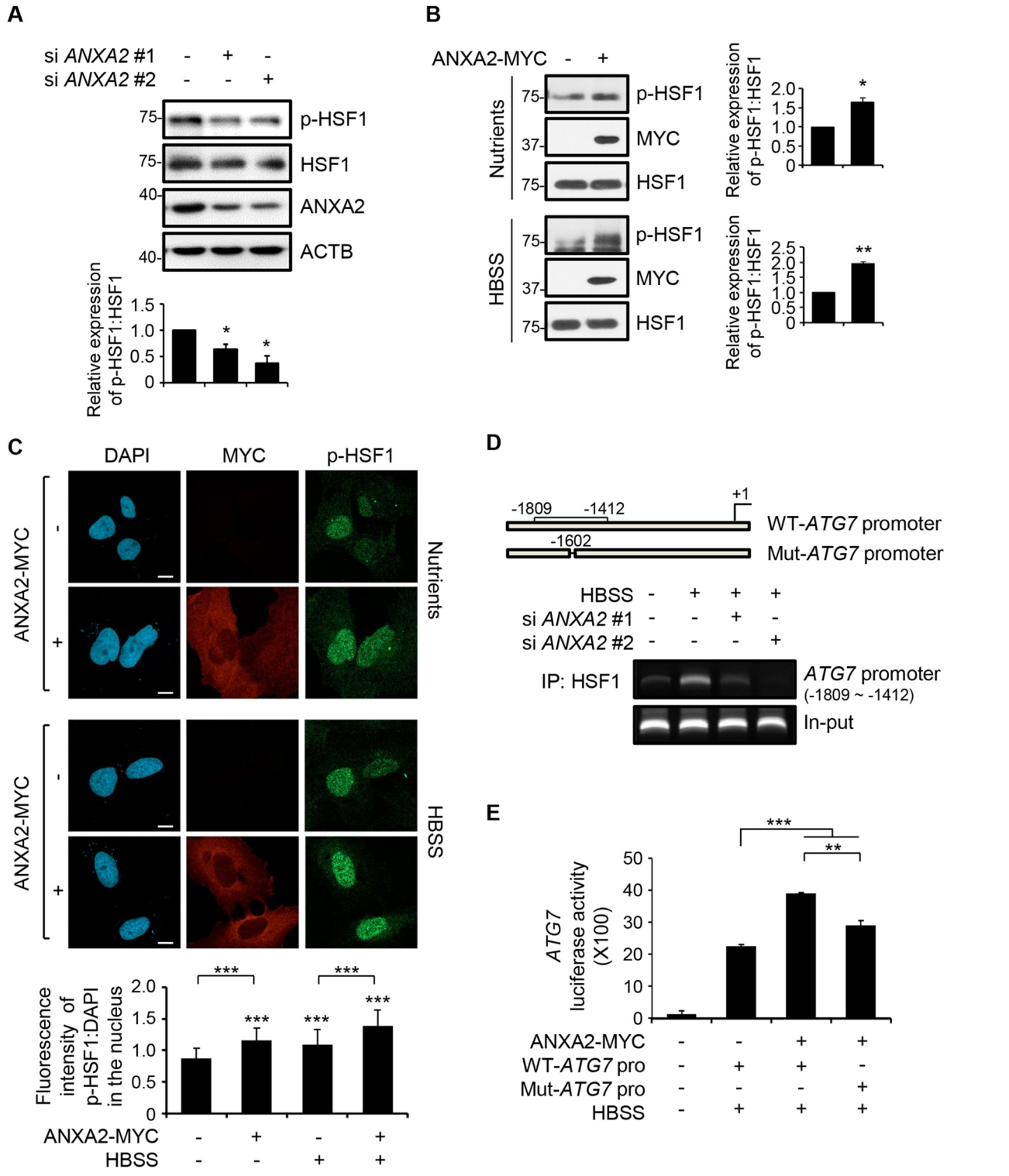

Figure 3. ANXA2 plays a key role in HSF1 (heat shock transcription factor 1)-induced transcription of ATG7. (A) Hs578T cells were transiently transfected with two siRNAs targeting *ANXA2* (+) or scrambled siRNA as a control (-). Immunoblot analysis was conducted. The relative band intensities of p-HSF1 were quantified by densitometry and normalized to HSF1. (B) Hs578T cells were transfected with plasmid expressing ANXA2-MYC (+) or empty plasmid (-), and the cells were cultured in growth medium or starved in HBSS for 2 h. Immunoblot analysis was conducted. The relative band intensities of p-HSF1 were quantified by densitometry and normalized to HSF1. (C) Representative images were shown the cellular distributions of p-HSF1 in Hs578T cells expressing ANXA2-MYC or empty vector. The cells were starved in HBSS for 2 h and immunostained with anti-p-HSF1 and anti-MYC antibodies shown in green and red, respectively. DNA was stained by DAPI. The mean fluorescence intensity of p-HSF1 within the nucleus was measured and normalized to the mean fluorescence intensity of DAPI per cell from 30 independent images. Scale bar of images: 10 μm. (D) ChIP assay was performed to measure the binding degree of HSF1 to the *ATG7* promoter in Hs578T cells. The schematic diagram indicates the wild type *ATG7* promoter (WT-*ATG7* promoter, top) and mutant *ATG7* promoter (mut-*ATG7*-promoter, deletion of consensus HSF1 binding site at − 1602, bottom). Hs578T cells transfected with scrambled siRNA (-) or siRNA molecules #1 and #2 targeting *ANXA2* (+) were starved in HBSS for 2 h. Chromatin was immunoprecipitated with specific antibodies against HSF1. DNA was amplified by PCR using primers covering the binding site for HSF1 in the *ATG7* promoter (−1809 to − 1412) and separated on 1% agarose gel. The relatively increased band intensity indicates that the binding of HSF1 protein to *ATG7* promoter is increased. (E) The effect of HSF1 on *ATG7* promoter activity was detected by luciferase reporter assay. Hs578T cells expressing ANXA2-MYC or empty vector were transfected with WT or mut *ATG7* promoter plasmid. The cells were starved with HBSS for 2 h and the firefly luciferase activity was measured and normalized to Renilla luciferase activity. Data represent mean ± S.E. (unpaired two-tailed Student's *t*-test). *,**,*** statistically significant at $p < 0.05$, $p < 0.01$, and $p < 0.001$ respectively. All data were representative of the results of three independent experiments.

the region from −1809 to −1412, including the identified HSF1 binding region (from −1602 to −1570) [30], as evidenced by ChIP assay (Figure 3D). The increased binding of HSF1 to the *ATG7* promoter was inhibited by ANXA2 silencing. In order to demonstrate the impact of the direct binding of HSF1 to the *ATG7* promoter, we conducted a luciferase reporter assay. We generated a mutant *ATG7* promoter in which the HSF1 consensus-binding site (at −1602) was deleted [30]. Overexpression of ANXA2 led to a significant increase in *ATG7* promoter luciferase expression compared to the control (Figure 3E). The mutation in the *ATG7* promoter significantly reduced luciferase expression compared to the wild-type, which is consistent with previous findings. These results strongly supported the crucial role of HSF1 in facilitating the transcriptional activation of the *ATG7* gene in the context of ANXA2-mediated autophagy induction.

Analysis of human breast tumor tissues from forty-three breast cancer patients in GEO dataset (GSE15852) showed a positive correlation between ANXA2 and LC3B with a Pearson correlation coefficient of 0.5252 ($n = 43$, $p = 0.0003$, Fig. S2C). ANXA2 showed a positive correlation with ATG7, as indicated by a Pearson correlation coefficient of 0.3230 ($n = 43$, $p = 0.0346$, Fig. S2D), suggesting a close relationship between ANXA2 and autophagy in breast cancer patients.

MTORC2 is important for ANXA2-mediated ATG7 transcription by HSF1

To identify the signaling pathway(s) responsible for ANXA2 regulation, MTOR pathway was examined, as it has previously been reported to be closely associated with autophagy [34]. MHY1485 is a selective MTOR activator that targets the ATP domain of MTOR [35], resulting in MTORC1 (p-RPS6KB/p70S6K) and MTORC2 (p-MTOR [S2481]) pathway activation (Fig. S5). Treatment with MHY1485 increased the protein expression of ANXA2, ATG7 and p-HSF1 (Figure 4A), suggesting that MTOR activation by treatment MHY1485 may be aligned to p-HSF1-ATG7 signaling in TNBC cells.

ANXA2 expression was significantly reduced by silencing MTOR and RICTOR (a component of MTORC2); however, it was not changed when RPTOR/Raptor (a component of MTORC1) was inhibited (Figure 4B). While MTOR pathway regulated the protein level of ANXA2, the mRNA level was not affected by knockdown of MTOR, RPTOR, or RICTOR (Fig. S6A and S6B). Treatment with rapamycin, which is a known inhibitor of MTORC1 [34], effectively inhibited phosphorylation of RPS6KB/p70S6K and did not alter the protein level of ANXA2 (Fig. S6C). The knockdown of RICTOR by two siRNA molecules inhibited the bafilomycin A_1-induced LC3B-II accumulation (Figure 4C). RICTOR silencing reduced the protein and mRNA level of *ATG7* (Figure 4C,D), suggesting that MTORC2 may affect autophagy through the translational regulation of ANXA2, independently of the MTORC1 pathway.

Knockdown of RICTOR significantly decreased the phosphorylated form of HSF1 (Figure 4E). Starvation-induced binding of HSF1 to the promoter region of *ATG7* was inhibited by RICTOR depletion (Figure 4F). These data, when considered along with the results of ANXA2 silencing, which are shown in Figure 3D, supported that MTORC2 was crucial to ANXA2-mediated autophagy through the HSF1-induced transcription of *ATG7* in Hs578T TNBC cells.

MTORC2-HSPA pathway may protect ANXA2 from lysosomal degradation

As MTORC2 pathway was involved in the translational regulation of ANXA2, we next investigated the possible regulatory factor for ANXA2 protein stability. It has been reported that heat shock increases the cell surface expression of ANXA2 without affecting its mRNA [36]. Among heat shock proteins, the stress-induced chaperones HSPA/Hsp70 and HSP90 are critical in maintaining protein homeostasis [37]. Heat shock at 42°C significantly increased the protein expression of ANXA2 with concomitant increases in HSPA and HSP90A (Figure 5A). The knockdown of HSPA significantly decreased the protein levels of ANXA2, ATG7, and LC3B-II (Figure 5B), while the mRNA level of *ANXA2* remained unchanged (Fig. S6D). An HSPA inhibitor, VER155008 [38], decreased the protein level of ANXA2 (Figure 5C). By contrast, neither the HSP90A knockdown nor the HSP90 inhibitor 17-AAG [38] altered the protein level of ANXA2 (Fig. S6E and S6F, respectively). The data indicate that ANXA2 stability was regulated by HSPA but not HSP90A.

According to an algorithm for predicting DnaK binding sites in the amino acid sequence of ANXA2 (LIMBO software, http://limbo.switchlab.org [39]), there are seven potential binding sites for DnaK, a prokaryotic member of HSPA family. A co-immunoprecipitation analysis showed that HSPA interacted with ANXA2 (Figure 5D), suggesting that HSPA is a potential interacting protein with ANXA2, which may affect the stability of ANXA2 protein.

There are two major pathways for protein degradation in eukaryotic cells: ubiquitin-proteasome pathway and lysosomal proteolysis [40]. To investigate whether the lysosome system was involved in the degradation of ANXA2, Hs578T cells were treated with leupeptin, an inhibitor of lysosomal proteolysis [41]. The reduced ANXA2 level by HSPA silencing was recovered by leupeptin (Figure 5E). Treatment with leupeptin significantly restored the protein level of ANXA2, which was decreased by siRNA *RICTOR* (Figure 5F). Treatment with MG132, a proteasome inhibitor, did not significantly alter the protein level of ANXA2 (Fig. S6G) and failed to recover the RICTOR silencing-induced ANXA2 reduction (Fig. S6H). These results demonstrate that the ANXA2 degradation could not be attributed to the ubiquitin-proteasome system.

The HSPA protein level was significantly reduced by RICTOR silencing, while the knockdown of HSPA did not affect the protein level of RICTOR (Figure 5G). The data suggest that RICTOR may be an upstream regulator of HSPA. Taken together, these results suggest that MTORC2-HSPA pathway is important for ANXA2 stability by protecting it from lysosomal proteolysis.

To explore the correlation between ANXA2 and HSPA in human samples, the protein levels of ANXA2 and HSPA were analyzed in human breast cancer tissues and adjacent normal

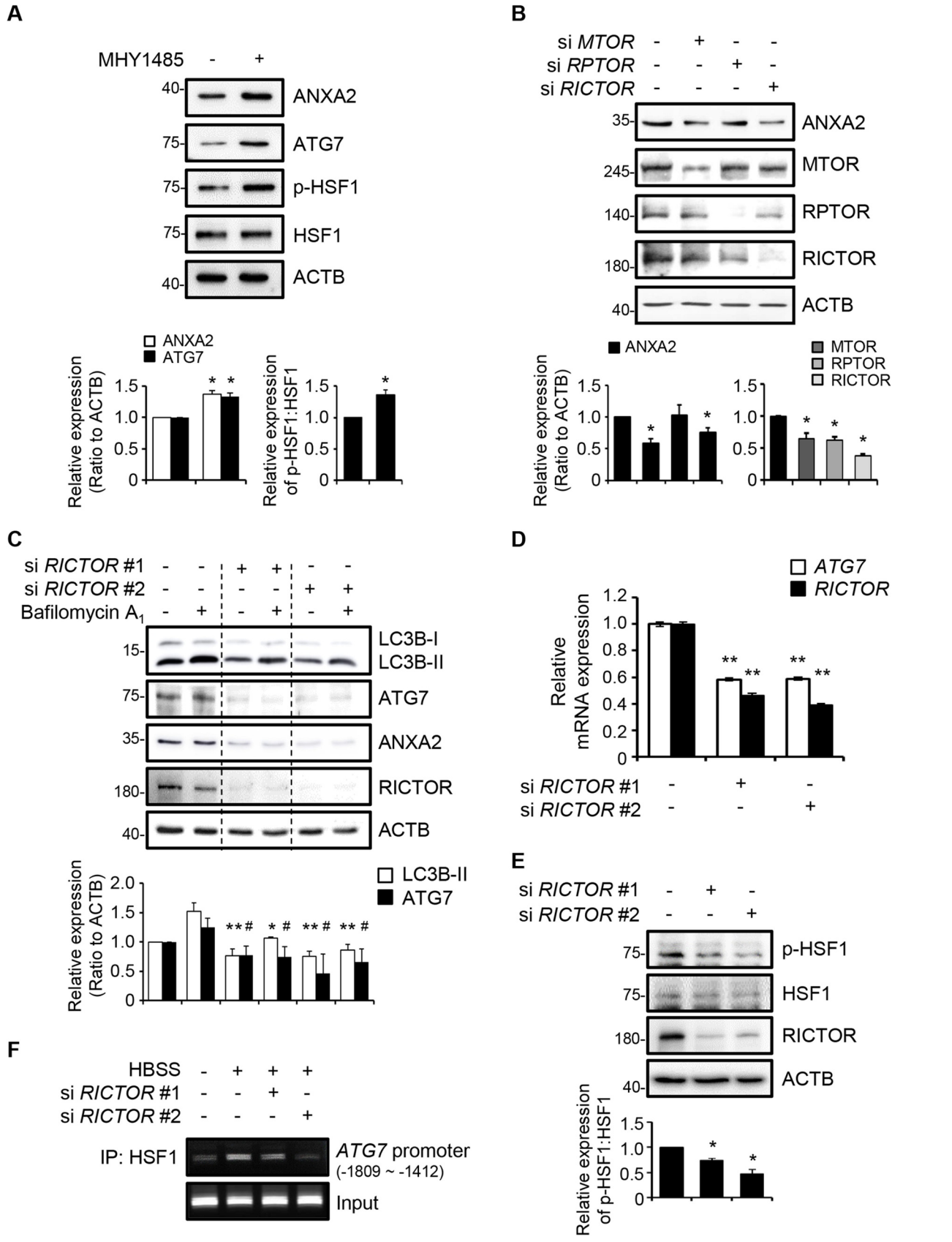

Figure 4. MTORC2 is important for ANXA2-mediated ATG7 transcription by HSF1. (A) Hs578T cells were treated with MHY1485 (1 μM) for 24 h. Immunoblot analysis was conducted. The relative band intensities were quantified by densitometry and normalized to ACTB or HSF1. * statistically significant at $p < 0.05$. (B) Hs578T cells were transfected with siRNA targeting *MTOR*, *RPTOR*, or *RICTOR* (+). Scrambled siRNA (-) was used as a control. The protein levels were detected by immunoblot analysis. The relative band intensities were quantified by densitometry and normalized to ACTB. * statistically significant at $p < 0.05$. (C) Hs578T cells were transfected with two siRNAs targeting *RICTOR* (+) or scrambled siRNA (-) as a control. Cells were starved in HBSS for 2 h and treated with bafilomycin A_1 (200 nM) for 2 h. Immunoblot analysis was conducted. The relative band intensities were quantified by densitometry and normalized to ACTB. *,** indicated statistical significance of the relative expression of LC3B-II vs control cells treated with bafilomycin A_1 (white bar) at $p < 0.05$ and $p < 0.01$, representatively. # indicated statistical significance

tissues from nine breast cancer patients. The protein levels of both ANXA2 and HSPA were found to be significantly increased in breast cancer tissues (C) compared to normal tissues (N) (p = 0.0489 and p = 0.0445, respectively) (Figure 5H, left). The relative expression (C/N) of ANXA2 was significantly correlated with that of HSPA, with a Pearson correlation coefficient of 0.774 at p = 0.014 (Figure 5H, right).

ANXA2 inhibition increases doxorubicin sensitivity in TNBC cells

Inducing autophagy has been associated with chemoresistance in chemotherapy. Targeting autophagy has proven to be an effective strategy for improving sensitivity to multiple drugs, including cisplatin and doxorubicin [42–45]. Doxorubicin is the first-line chemotherapeutic regimen for the treatment of TNBC [46,47]. However, many patients develop resistance to doxorubicin, which exhibits adverse effects [48]. Here, the effect of ANXA2 silencing in doxorubicin-induced cell toxicity was measured using an MTT assay. Knockdown of ANXA2 significantly increased doxorubicin sensitivity in Hs578T cells (Figure 6A). The LC3B-II level was enhanced by doxorubicin and reduced by ANXA2 depletion (Figure 6B). We also showed that the combination of doxorubicin with siRNA against *ANXA2* significantly increased PARP1 cleavage, which is a hallmark of apoptosis [49]. To provide additional evidence, we conducted flow cytometry analysis. When treated with doxorubicin alone, there was an increase in the proportion of apoptotic cells compared to the vehicle control (3.96% vs. 8.56%). ANXA2 silencing in combination with doxorubicin treatment further increased this proportion (11.74%, Figure 6C). These results suggest that the inhibition of autophagy by ANXA2 knockdown may increase the doxorubicin sensitivity in TNBC cells.

We next employed an ANXA2 inhibitor, A2ti-1, to explore its impact on doxorubicin sensitivity. Our results indicated that the treatment of A2ti-1 in combination with doxorubicin enhanced the effectiveness of doxorubicin in a dose-dependent manner (Figure 6D). These findings strongly suggest that ANXA2 inhibition may indeed contribute to the augmentation of doxorubicin sensitivity.

ANXA2 knockdown increases doxorubicin sensitivity and retards the tumor growth in the TNBC xenograft mouse model

The role of ANXA2 in the *in vivo* tumorigenicity of TNBC cells was examined using a xenograft mouse model with Hs578T TNBC cells. To this end, shRNA control (sh Ctrl) or shRNA *ANXA2* (sh *ANXA2*) expressing Hs578T cells were inoculated into the right mammary gland of female BALB/$C^{nu/nu}$ mice (n = 16 per group). As shown in Figure 7A, the tumor incidence rate of sh Ctrl Hs578T cells-injected group was 50%, while that of sh *ANAX2* Hs578T cells-injected group was 18.75%. ANXA2 knockdown tends to retard the growth of tumors, but not significant in a Hs578T TNBC xenograft model (Fig. S7A).

Next, we investigated if ANXA2 knockdown could enhance doxorubicin sensitivity *in vivo*. We established a TNBC xenograft mouse model using sh Ctrl or sh *ANXA2* MDA-MB-231 cells. Tumor-bearing mice were randomly assigned to four groups (n = 7 per group): sh Ctrl-PBS, sh Ctrl with doxorubicin treatment, sh *ANXA2*-PBS, sh *ANXA2* with doxorubicin treatment. Doxorubicin or PBS was intravenously administered once a week for 33 days.

First, we confirmed that ANXA2 knockdown reduced the expression of p-HSF1, ATG7, and LC3B-II in MDA-MB-231 cells (Fig. S7B and S7C). ANXA2 knockdown alone did not affect tumor growth and volume, but the combination of ANXA2 knockdown and doxorubicin administration significantly reduced tumor volume compared to doxorubicin treatment alone (Figure 7B–D). Moreover, the combination of ANXA2 knockdown with doxorubicin completely eliminated tumors in three mice. The body weights of the mice did not change in all four groups (Fig. S7D). The TUNEL assay showed an increased number of apoptotic nuclei in the tumor tissues derived from sh *ANXA2* group compared to tissues from sh Ctrl group. Furthermore, the level of TUNEL-positive cells was significantly higher in the tumor tissues from sh *ANXA2* with doxorubicin treatment group (Figure 7E). These results suggest that the inhibition of ANXA2 has a substantial impact on enhancing apoptosis and sensitizing doxorubicin treatment in the MDA-MB-231 xenograft tumor model.

Discussion

The annexin family has been reported to be linked to autophagy in the process of initiation of phagophores, the development of autophagosomes, and the fusion of autophagosomes with lysosomes [50]. Consistent with our data (Figure 1A,B), high levels of ANXA2 have previously been shown to be associated with poor overall survival and relapse-free survival of TNBC patients [22,51]. ANXA2 has contributed to the formation of autophagosomes containing ATG16L1, ATG9A, and ATG5 [23,24,50]. For the first time, the present study demonstrated that ANXA2 affected ATG7 expression, leading to increased autophagy flux in TNBC cells (Figures 1 and 2). ANXA2 did not regulate *LC3B* mRNA level using ANXA2 silencing and overexpressing cells (Data not

of the relative expression of ATG7 vs control cells treated with bafilomycin A_1 (black bar) at $p < 0.05$. (D) Hs578T cells were transfected with two siRNAs targeting *RICTOR* (+) or scrambled siRNA (-) as a control. The mRNA levels of *ATG7* and *RICTOR* were determined by qRT-PCR analysis. ** statistically significant at $p < 0.01$. (E) Hs578T cells were transfected with siRNA targeting *RICTOR* (+) or scrambled siRNA (-) as a control. Immunoblot analysis was conducted. The relative band intensities of p-HSF1 were quantified by densitometry and normalized to HSF1. * statistically significant at $p < 0.05$. (F) ChIP assay was performed to measure the binding degree of HSF1 to the *ATG7* promoter in Hs578T cells. Hs578T cells transfected with scrambled siRNA (-) or siRNA molecules #1 and #2 targeting *RICTOR* (+) were starved in HBSS for 2 h. Chromatin was immunoprecipitated with specific antibodies against HSF1. DNA was amplified by PCR using primers covering the binding site for HSF1 in the *ATG7* promoter (−1809 to − 1412) and separated on 1% agarose gel. The relatively increased band intensity indicates that the binding of HSF1 protein to *ATG7* promoter is increased. Data represent mean ± S.E. (unpaired two-tailed Student's *t*-test). All data were representative of the results of three independent experiments.

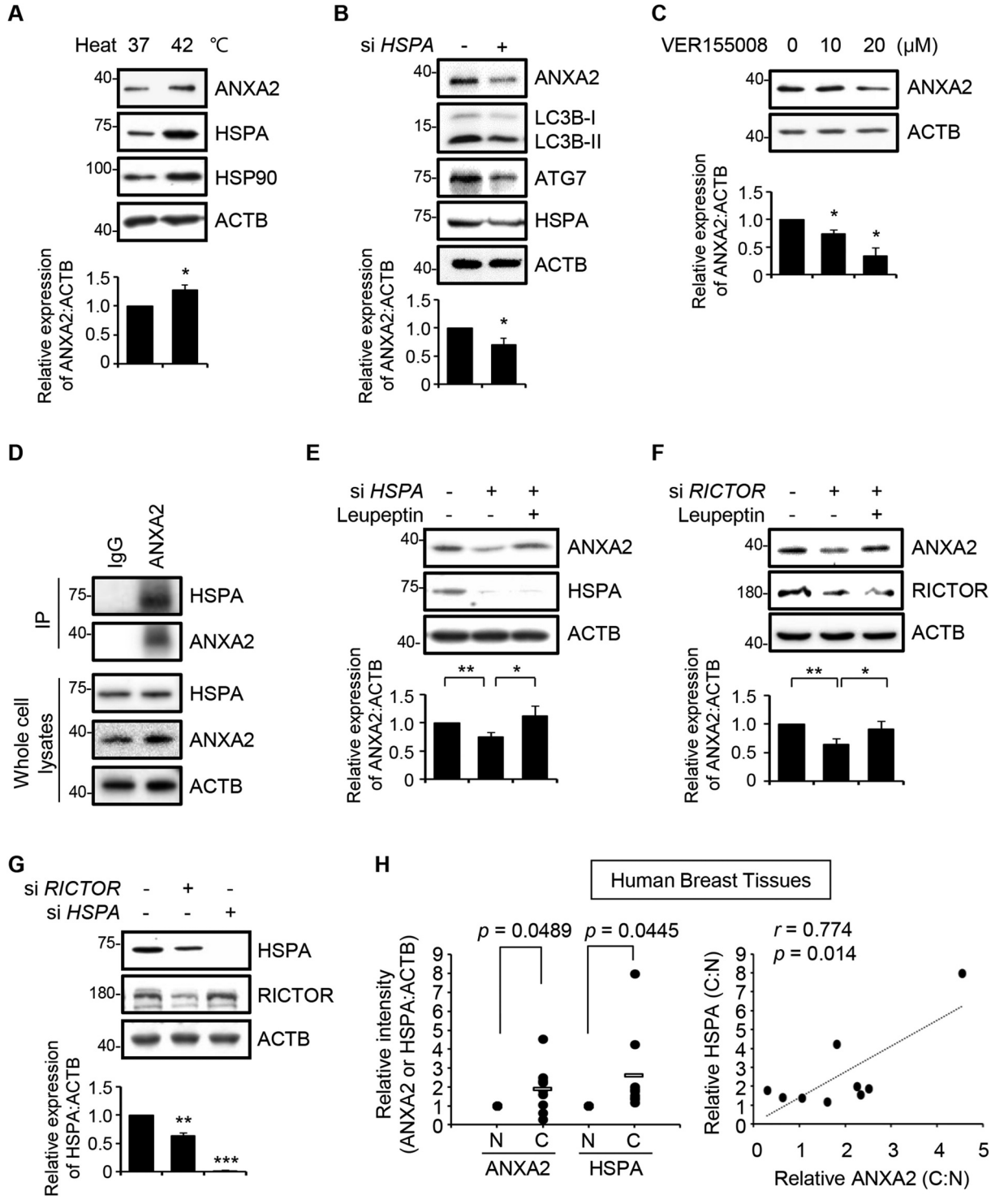

Figure 5. MTORC2-HSPA pathway may protect ANXA2 from lysosomal degradation. (A) Hs578T cells were heated (42°C for 3 h) and then incubated at 37°C for 24 h. Immunoblot analysis was conducted. The relative band intensities of ANXA2 were quantified by densitometry and normalized to ACTB. (B) Hs578T cells were transfected with siRNA targeting *HSPA* (+) or scrambled siRNA (-) as a control. Immunoblot analysis was conducted. The relative band intensities of ANXA2 were quantified by densitometry and normalized to ACTB. (C) As indicated, Hs578T cells were treated with VER155008 for 24 h. Immunoblot analysis was subjected. The relative band intensities of ANXA2 were quantified by densitometry and normalized to ACTB. (D) Whole cell lysates of Hs578T cells were immunoprecipitated with anti-ANXA2 antibody and immunoblotted with anti-HSPA antibody. (E and F) Hs578T cells were transfected with siRNA targeting *HSPA* (+, E), siRNA targeting *RICTOR* (+, F) or scrambled siRNA (-) as a control. The cells were treated with 50 μg/mL leupeptin for 24 h and subjected to immunoblot analysis. The relative band intensities of ANXA2 were quantified by densitometry and normalized to ACTB. (G) Hs578T cells were transfected with siRNA targeting *RICTOR* (+) or siRNA targeting *HSPA* (+). Scrambled siRNA (-) was used as a control. Immunoblot analysis was conducted. The relative band intensities of HSPA were quantified by densitometry and normalized to ACTB. (H) Quantification of immunoblot band densities for ANXA2 and HSPA which were normalized to ACTB in nine pairs of human breast cancer tissues (C) and adjacent normal tissues (N) from immunoblot analysis (left). Bars indicate average values ($n = 9$; unpaired two-tailed Student's *t*-test). Pearson correlation coefficient (two-tailed Student's *t*-test) between ANXA2 and HSPA protein expression (right). Data represent mean ± S.E. (unpaired two-tailed Student's *t*-test). *,**,*** statistically significant at $p < 0.05$, $p < 0.01$, and $p < 0.001$. All data were representative of the results of three independent experiments.

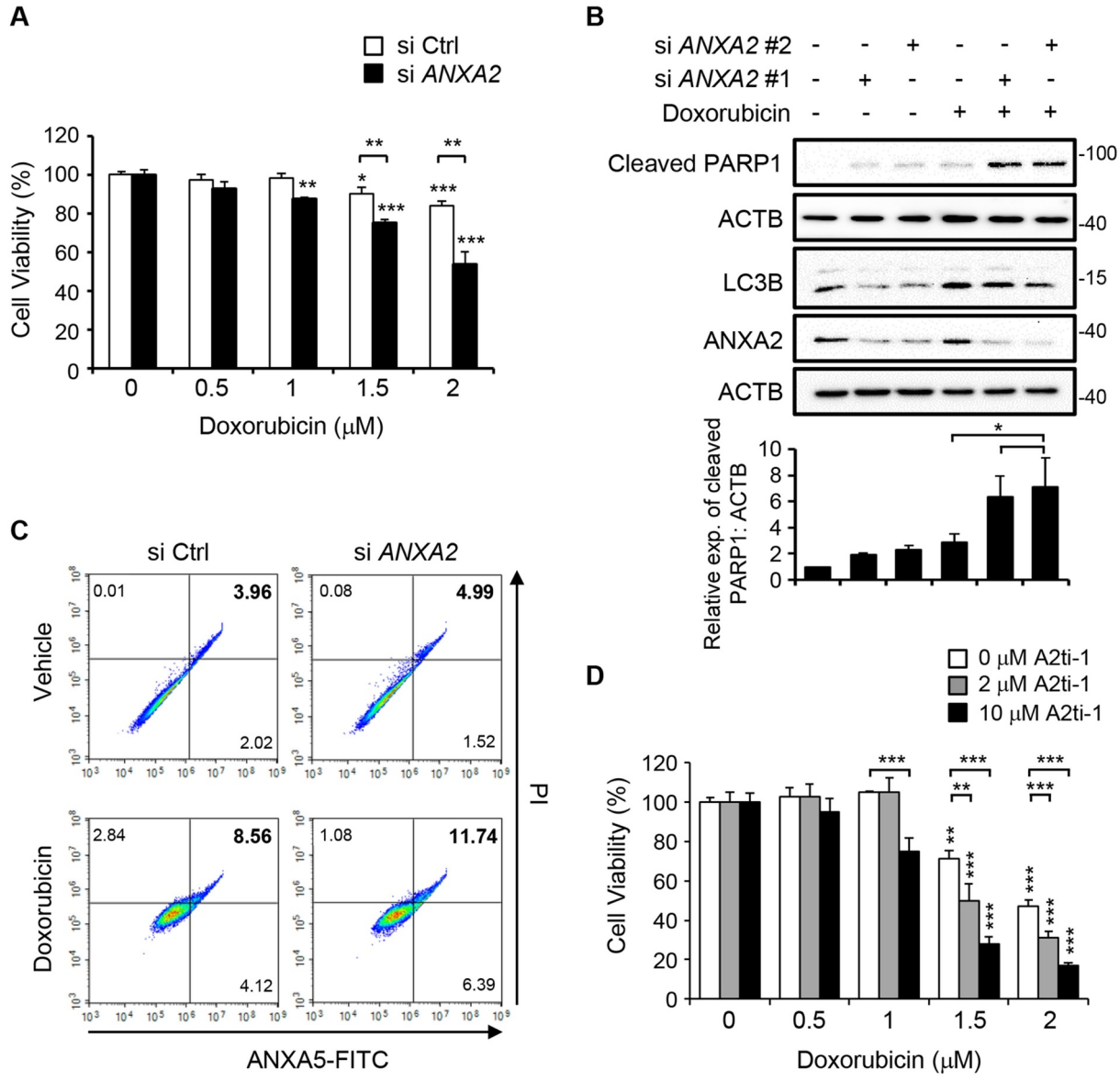

Figure 6. ANXA2 knockdown increases doxorubicin sensitivity in TNBC cells. (A) Hs578T cells were transfected with siRNA targeting *ANXA2* (+) or scrambled siRNA (-) as a control. The cells were treated with doxorubicin (0, 0.5, 1, 1.5, and 2 μM) for 24 h and subjected to MTT assay. (B) Hs578T cells were transfected with two siRNAs targeting *ANXA2* (+) or scrambled siRNA (-) as a control. The cells were treated with 1 μM doxorubicin for 24 h and subjected to immunoblot analysis. Immunoblot analysis was conducted. The relative band intensities of cleaved PARP1 were quantified by densitometry and normalized to ACTB. (C) Flow cytometry results with ANXA5-FITC and PI staining. Hs578T cells were transfected with siRNA targeting *ANXA2* or scrambled siRNA, and treated with 2 μM doxorubicin. After culture for 24 h, the cells were harvested and stained using ANXA5-FITC and PI. The apoptosis was analyzed by flow cytometry. (D) Hs578T cells were treated with A2ti-1 and doxorubicin for 24 h, as indicated concentration. MTT assay was conducted. Data represent mean ± S.E. (unpaired two-tailed Student's *t*-test). *,**,*** statistically significant at $p < 0.05$, $p < 0.01$, and $p < 0.001$. All data were representative of the results of three independent experiments.

shown). ANXA2 has been reported to be critical for osteosarcoma cell autophagy and subsequent cell differentiation [52]. The binding of ANXA2 with bleomycin impedes autophagic flux, leading to the induction of pulmonary fibrosis progression [53]. The significant function of ANXA2 in the proliferation and invasion of TNBC cells [17–20], along with its correlation with advanced clinical stage of invasive breast cancer [20,22], implies that ANXA2-mediated autophagy may contribute to a prosurvival role in TNBC.

The ATGs are required for various stages of autophagy whose functions in cancer are context-dependent. The ATG7-dependent autophagy has been shown to be involved in invasion in human bladder cancer [54]. The role of ATG7 in breast cancer progression has been controversial. A high level of ATG7 has been shown to be correlated with a worse survival rate in breast cancer and TNBC patients [30], but it inhibits proliferation/migration and promotes apoptosis in TNBC cell lines [55]. While a close association between TNBC and ATG7 has been reported [30], the intricate mechanistic relationship between ATG7 and ANXA2 in TNBC has not yet been studied. The current study showed that ANXA2 regulated ATG7 to induce autophagy *via* HSF1 in a transcriptional level (Figures 2 and 3). The previous study shows that ANXA2 knockdown decreases the levels of ATG16L1 and ATG12–ATG5 [23]. ANXA2 did not cause substantial alterations in the mRNA levels of *ATG4B*, *ATG5*,

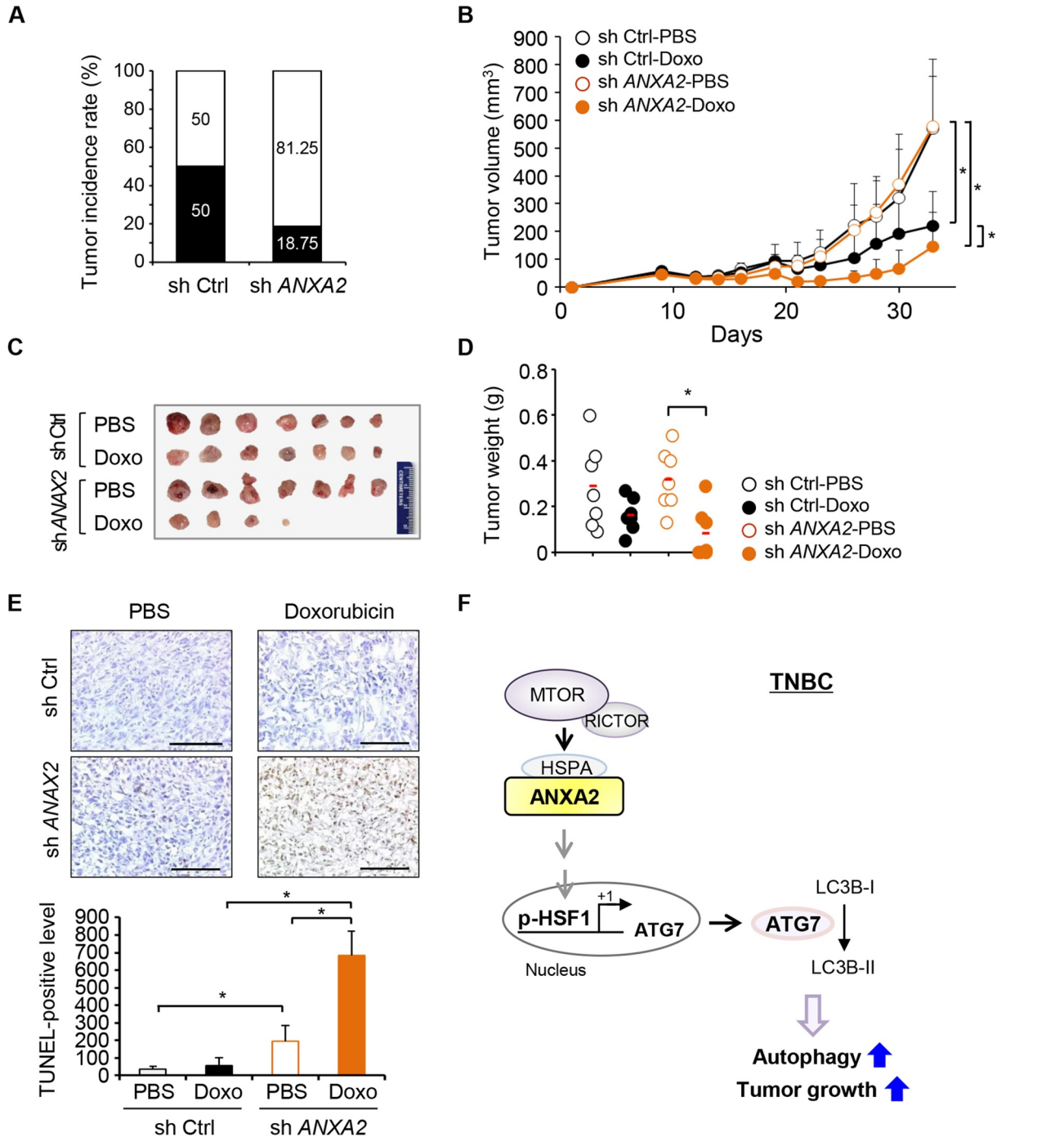

Figure 7. ANXA2 knockdown increases doxorubicin sensitivity and retards the tumor growth in the TNBC xenograft mouse model. (A) Hs578T cells stably transfected with shRNA targeting *ANXA2* (sh *ANAX2*) or scrambled shRNA (sh Ctrl) were inoculated to Balb/c nude mice ($n = 16$ per group). The tumor incidence was calculated as the ratio of tumor-bearing mice (n) to total mice (n) for 17 days. The numbers in bars indicate the percentage of mice (black bar: the mice which developed tumors, white bar: the mice which did not develop tumors). (B-D) MDA-MB-231 cells stably transfected with shRNA targeting *ANXA2* (sh *ANAX2*) or scrambled shRNA (sh Ctrl) were inoculated to Balb/c nude mice ($n = 7$ per group). Tumor-bearing mice were randomized into four groups: control group (sh Ctrl-PBS), doxorubicin-treated group (sh Ctrl-doxo), ANXA2 knockdown group (sh *ANXA2*-PBS), and combination of ANXA2 knockdown and doxorubicin-treated group (sh *ANXA2*-doxo). Doxorubicin (3 mg/kg) or vehicle (PBS) was intravenously administered once a week for 33 days. Tumor volume was measured three times per a week using caliper (B). At the end of the study, animals were sacrificed. The excised tumors were obtained (C) and tumor weight was measured (D). * statistically significant at $p < 0.05$ (two way ANOVA followed by Tukey test). (E) TUNEL assay was performed using tumor tissues obtained from the mice in four groups. Apoptotic cells were stained as brown spots in the tissues and representative images were shown (scale bar = 100 μm). TUNEL-positive levels in the tissue were analyzed by Image J software. * statistically significant at $p < 0.05$ (two way ANOVA followed by Tukey test). (F) A proposed mechanism for the MTORC2-ANXA2-HSF1-ATG7 axis which plays a key role in autophagy of TNBC cells.

and *ATG12* in Hs578T TNBC cells (Data not shown). In the current study, we showed that the expression of ATG7 displayed a significant change in response to ANXA2. There may be the potential involvement of other molecules in the regulation of autophagosome formation by ANXA2 in TNBC.

The high levels of ATG7 [30] and nuclear HSF1 [56] have been associated with poor survival in breast cancer patients. The positive correlation between HSF1 and ATG7 levels in these patients further supports our *in vitro* findings. Our results imply that HSF1 located in nucleus of TNBC cells was phosphorylated by ANXA2, which stimulated the ATG7 promoter activity and induced autophagy. It has been demonstrated that TFE3 and TFEB, nutrient-sensitive transcription factors, induce transcriptional upregulation of autophagic and lysosomal genes in response to starvation, playing a master regulatory role in autophagy [57]. Although MTOR regulates the translocation of TFEB to regulate autophagy [58], TFEB does not appear to affect ATG7 expression in HeLa cells [59]. In our study, we demonstrated that ANXA2 played a role in p-HSF1-ATG7 signaling under both nutrient-rich and starvation conditions. As ANXA2 is involved in TFEB-mediated autophagy [52,53], we cannot exclude the potential involvement of TFEB and TFE3 in the regulation of ANXA2-dependent autophagy in TNBC, as well as their potential crosstalk with HSF1.

Many studies have focused on the regulatory signals of MTORC1 activity on autophagy [34]; however, the mechanism of MTORC2 regulation in autophagy is yet to be fully understood. Current studies have suggested that MTORC2 functions as a multifaceted regulator of autophagy *via* complicated signaling network. With the activation of its downstream target molecules SGK1 (serum/glucocorticoid regulated kinase 1) and AKT, MTORC2 functions as a negative regulator of autophagy [60]. Otherwise, the MTORC2- PRKCA (protein kinase C alpha)/PRKCB axis facilitates autophagosome precursor formation, thus promoting autophagy [61]. In this paper, we demonstrated that MTORC2-regulated ANXA2 promoted autophagy through HSF1-mediated ATG7 in TNBC cells (Figure 4). Consistently, MTORC2 signaling activates HSF1 *via* a positive feedback loop in glioblastoma cells [62].

It has been reported that phosphorylated MTOR interacts with ANXA2, causing a shift in its subcellular location from the periphery of the plasma membrane to the perinuclear region, thereby inducing autophagy under serum starvation [25]. The downstream signaling of MTORC2, including p-AKT (S473) and PRKCA/PKCα, appeared to have differential effects on ANXA2 expression. An AKT inhibitor, MK2206, reduced ANXA2 expression, while a PRKC inhibitor, Gö 6983, did not induce any significant change (Data not shown). Our findings suggest that MTORC2 complex signaling modulates autophagy, including the regulation of ANXA2.

Heat shock-induced HSP90A enhances ANXA2 interaction with S100A10, which results in the formation of heterotetramer and extracellular translocation [63]. Our data demonstrated that HSPA interacted with ANXA2, and this interaction may be crucial for the protein stability of ANXA2, thus preventing lysosomal degradation (Figure 5). We also observed a positive correlation between HSPA and ANXA2 in human breast cancer tissues. Our data imply that the interaction between ANXA2 and HSPA may affect the expression, subcellular localization, and functional implication of ANXA2 in breast cancer. The impact of HSF1 on HSPA expression aligns well with our study's evidence of the ANXA2-HSPA interaction.

A number of studies have reported crosstalk between apoptosis and autophagy, thereby providing a rationale for the inhibition of autophagy in conjunction with apoptosis-inducing therapies in human cancers [64,65]. A high level of basal autophagy in TNBC cells has been shown to be correlated with poor prognosis [10,13,14]. The inhibition of autophagy sensitizes the effects of chemotherapeutic drugs in breast cancer [11,12]. Thus, targeting of ANXA2-mediated autophagy has been suggested to be an attractive approach for aggressive breast cancer therapy [10,66]. Although there has been evidence showing that doxorubicin induces autophagy in TNBC cells [42], the correlation between doxorubicin-induced apoptosis and autophagy remains unclear. This study showed that the inhibition of autophagy by knockdown of ANXA2 markedly increased doxorubicin sensitivity in TNBC cells *in vitro* (Figure 6). We verified the inhibition of tumorigenicity by knockdown of ANXA2 using a Hs578T TNBC xenograft model. Notably, ANXA2 knockdown in combination with doxorubicin treatment increased apoptotic cell death and retarded tumor volume compared to doxorubicin treatment alone in a MDA-MB-231 TNBC xenograft model (Figure 7). These results highlighted the significance of targeting ANXA2 in enhancing doxorubicin sensitivity, presenting a promising approach to improve chemotherapy effectiveness in TNBC.

Taken together, the results of the present study demonstrated a mechanism for autophagy in TNBC cells wherein MTORC2-ANXA2-HSF1-ATG7 axis played a key role (as depicted in Figure 7F). Herein, our data showed that MTORC2-regulated ANXA2 increased the transcription of the *ATG7* gene through HSF1, thereby inducing autophagy. We also showed that HSPA, which interacted with ANXA2, enhanced ANXA2 protein stability. Collectively, our study provides novel insights into ANXA2-mediated autophagy in TNBC, suggesting that ANXA2 is a potential therapeutic target against aggressive breast cancer.

Materials and methods

Cell culture conditions and reagents

Hs578T and MDA-MB-231 human TNBC cell lines were purchased from the Korean Cell Line Bank (30126 and 30026, respectively). All cell lines were cultured in Dulbecco's Modified Eagle's Medium (DMEM) with high glucose (Hyclone, SH30243.01) supplemented with 10% fetal bovine serum (Corning, 35–015-CV) and 1% penicillin-streptomycin (Invitrogen, 15140–122) at 37°C in a humidified incubator equilibrated with 5% CO_2. All cell lines were authenticated by the Korean Cell Line Bank using STR-PCR analysis. Bafilomycin A_1 (Sigma Aldrich, B1793), Hanks' balanced salt solution (HBSS; Sigma Aldrich, H8264), rapamycin (Sigma Aldrich, R8781), VER155008 (Sigma Aldrich, SML0271), MG132 (Sigma Aldrich, C2211), and

MHY1485 (Sigma Aldrich, SML0810), leupeptin HCl (Calbiochem 108,975), A2ti-1 (MedChemExpress, HY-136465), and doxorubicin (Sigma Aldrich, D1515) were used as indicated. To induce autophagy, cells were starved by incubation in HBSS medium lacking amino acid and serum for 2 h [31].

Immunoblot analysis

Immunoblot analysis was performed as described previously [67] and the following primary antibodies were used: Anti-RPTOR (Santa Cruz Biotechnology [SCB], sc-81537), anti-HSPA/Hsp70 (SCB, sc-66048), anti-ANXA2 (SCB, sc-28385), anti-ACTB (SCB, sc-47778), anti-TUBA (SCB, sc-23948), anti-MTOR (Cell Signaling Technology [CST], 2972S), anti-phospho-MTOR (Ser2448) (CST, 2971S), anti-phospho-MTOR (Ser2481) (CST, 2974S) and anti-LC3B (CST, 2775S), anti-ATG7 (CST, 8558S), anti-HSF1 (CST, 12972S), anti-RICTOR (Abcam, ab70374), ati-SQSTM1/p62 (Abcam, ab56416), anti-phospho-HSF1 (S326) (CUSABIO, CSB-RA010791A326phHU), anti-HSP90A/Hsp90α (Enzo Life Sciences, ADI-SPA-840), anti-phospho-RPS6KB/p70 S6 kinase (Thr389) (CST, 9205S), anti-RPS6KB/p70 S6 kinase (CST, 9202S), anti-TFE3 (Proteintech, 14480–1-A), and anti-TFEB (SCB, sc-166736) antibodies. An enhanced chemiluminescence system (Advansta, R-03031-D25) was used for detection. The relative band intensities were quantified by densitometry and normalized to loading control protein.

RFP-GFP-LC3 puncta formation assay

Hs578T cells were transiently transfected with the tandem reporter RFP-GFP-LC3 using Omicsfect (OmicsBio, CP2101) and serum-free DMEM medium (Welgene, LM001–05) for 24 h. To induce starvation, the cells were maintained in HBSS (Sigma Aldrich, H8264) for 2 h. The coverslips were mounted on glass slides. Immunofluorescence was performed using a LSM 900 confocal laser scanning microscope (Carl Zeiss). RFP-GFP-LC3 puncta were counted. The number of RFP^+ GFP^+ LC3 dots (yellow puncta) and the number of RFP^+ GFP^- LC3 dots (red puncta) in the merged images were counted and the average number of puncta per cell was calculated.

Confocal fluorescence microscopy

Hs578T cells, which were seeded, were fixed with 4% paraformaldehyde for 10 min, washed with phosphate-buffered saline (PBS; 1.37 mM sodium chloride, 27 mM potassium chloride, 100 mM sodium phosphate dibasic, 18 mM potassium phosphate monobasic, pH 7.4), and then permeabilized with PBS containing 0.2% Triton X-100 (Biopure Corporation, 8940T) for 5 min at room temperature. After washing with PBS, the cells were blocked for 30 min in PBS containing 2% bovine serum albumin (BSA; GenDEPOT, A0100–010). The cells were then incubated with the indicated primary antibody (1:200–1:400) overnight at 4°C, washed, and stained for 1 h with Alexa Fluor 488 (Invitrogen, A11034) and Alexa Fluor 568 (Invitrogen, A11031)-conjugated secondary antibodies. 4-, 6-diamidino-2-phenylindole (DAPI) was used for nuclear staining. The coverslips were mounted on glass slides. Immunofluorescence was performed using a LSM 900 confocal laser scanning microscope (Carl Zeiss).

Quantitative reverse-transcription polymerase chain reaction

Total RNAs were extracted and reverse transcription was performed as described previously [67]. The qPCR (StepOne™ Real-Time PCR System, Thermo Scientific) reactions were performed using SensiFAST™ SYBR® Hi-ROX kit (Bioline Reagents, BIO-92005) with gene-specific primers: *ANXA2* (forward: 5'-GCCATCAAGACCAAAGGTGT-3', reverse: 5'-TCAGTGCT GATGCAAGTTCC-3'), *ATG7* (forward: 5'-GCCAAGATC TCCTACTCCAATC-3', reverse: 5'-CAGAAGTAGCAG CCAAGCTTGT-3'), and *RICTOR* (forward: 5'-GGAAGCCTGTTGATGGTGAT-3', reverse: 5'-GGCAGCCTGTTTTATGGTGT-3'). Each sample was assayed in triplicate.

Small interfering RNAs (siRNAs) and plasmid DNA transfection

The siRNA molecules targeting *MTOR* (HSS103826), *RPTOR* (HSS126373), and *RICTOR* (HSS153834) were obtained from Invitrogen. The siRNA molecules targeting *HSP90A* (sc-29353) were provided by Santa Cruz Biotechnology. Knockdown of HSPA was performed with siRNA targeting *HSPA*, 5'-AGGACGAGUUUGAGCACAA-3'. Knockdown of ANXA2 #1 and #2 were performed with siRNA targeting *ANXA2*, 5'-GGGUCUGUCAAAGCCUAUATT-3' and 5'-GCACUGAAGUCAGCCUUAUTT-3'. The ANXA2-MYC plasmid was obtained from Origene (RC205081). Cells cultured in 6-well plate were transfected using OPTI-MEM reduced-serum medium (Gibco, 51985034) and Lipofectamine 2000 (Invitrogen, 11668019) or jetPRIME® transfection reagent (Polyplus, 101000046) for 48 h.

Small hairpin RNA (shRNA) targeting ANXA2

An shRNA molecule targeting *ANXA2* (sc-29199-SH) and control shRNA (sc-108060) were purchased from Santa Cruz Biotechnology. Cells cultured in a 6-well plate were transfected using Lipofectamine 2000 (Invitrogen, 11668019) and OPTI-MEM reduced-serum medium (Gibco, 51985034), following the manufacturer's instruction. Transfected cells were selected with 2.5 μg/ml puromycin (Sigma Aldrich, P9620) for three weeks.

ATG7 promoter luciferase assay

Hs578T cells expressing ANXA2-MYC or vector were transiently co-transfected with the Renilla reporter and the wild-type or mutant *ATG7* promoter luciferase reporter as previously described [67]. The wild-type *ATG7* and mutant *ATG7* promoter was cloned within BglII and KpnI sites in pGL3 promoter as previously reported [30]. The HSF1

consensus-binding site (GAAACTTC, at-1602) in *ATG7* promoter was deleted using the site-directed mutagenesis approach with primers: 5'-GGTGAGAATTACAAATTAAG GGTGGGGGAGACT-3' (forward), 5'-AGTCTCCCCCAC CCTTAATTTGTAATTCTCACC-3' (reverse). After transfection for 24 h, the luciferase activity was assayed using the dual-luciferase reporter assay kit (Promega, E1910). The firefly luciferase activity was measured with a luminometer (Tecan, Infinite M Plex), which was normalized to Renilla luciferase activity.

Chromatin-immunoprecipitation (ChIP)

ChIP assay was performed as described previously [67]. Cells were subjected to knockdown using two siRNA molecules targeting *ANXA2* or *RICTOR* for 48 h, and then were starved in HBSS for 2 h. Chromatin DNA captured by 2 μg anti-HSF1 antibody (CST, 12972), were eluted from Protein G Agarose (Thermo Fisher Scientific, 20397) and DNA was extracted with TRIzol™ Reagent (Invitrogen, 15596026). The DNA fragments were amplified by PCR using primers covering the HSF1 binding site within the *ATG7* promoter (−1809 to −1412). The primer sequences were as follows: 5'-GTCAGCAAAGGGTGGTGGGATTATC-3' (forward), and 5'- AGCAACTGAAGATCCGCAGAAGTG-3' (reverse). Equal volumes of each RT-PCR product were analyzed by 1% agarose gel electrophoresis. Each sample was assayed in triplicate.

Co-immunoprecipitation

Co-immunoprecipitation was performed as described previously [67]. Whole cell lysates were incubated with 2 μg anti-ANXA2 antibody (SCB, sc-28385) overnight at 4°C. Protein G Agarose (Thermo Fisher Scientific, 20397) was added, resolved on SDS polyacrylamide gels, and immunoblotted with anti-HSPA antibody (SCB, sc-66048).

Flow cytometry analysis

Hs578T cells were transfected with siRNA targeting *ANXA2* or scrambled siRNA. The transfected cells were treated with 2 μM doxorubicin for 24 h. The cells were harvested and washed twice with PBS. Subsequently, the cells (1×10^5 cells) were stained with FITC Annexin V Apoptosis Detection Kit I (BD Biosciences, 556547) for 15 min at room temperature in 1X binding buffer. The stained cells were then analyzed using a Novocyte Flow Cytometer (ACEA Biosciences Inc.).

Cell viability assay

Hs578T cells were incubated in 96-well plate (5×10^3 cells/well) for 24 h. Cells were transfected with siRNA targeting *ANXA2* or scrambled siRNA. Then, the transfected cells were treated with doxorubicin and dimethyl sulfoxide (DMSO; Sigma Aldrich, D2650) for 24 h, followed by 2 h incubation with 1 mg/ml MTT (Sigma Aldrich, M5655). Cells were treated with doxorubicin and A2ti-1 for 24 h, followed by 2h incubation with 10 μL of CCK-8 assay reagent (Dojindo, CK04) per well. Following removal of the culture medium, the cells were dissolved in DMSO and shaken for 10 min. The absorbance was read measured at 450 nm using enzyme-linked immunosorbent assay plate reader (BioTek Instruments Inc., Synergy 2).

Xenograft tumor mouse model carrying shRNA ANXA2 Hs578T cells

Female Balb/c nude mice (5-weeks old, female) were obtained from JUNGAH BIO (Gyeonggi, Korea). The mice were handled using a protocol approved by Duksung Women's University in accordance with the Guidelines for the Care and Use of Laboratory Animals. All animal experiments were carried out in the animal laboratory of Duksung Women's University. Mice were acclimatized for 1 week before the experiment. Scrambled shRNA (sh Ctrl) or shRNA *ANXA2* (sh *ANAX2*) transfected Hs578T cells (5×10^6 cells/mouse) were orthotopically injected with 100 μl PBS solution containing 10% matrigel (Corning, 354262) into the right mammary fat pad of each mouse. Mice were randomly divided into two groups ($n = 16$ per group): sh Ctrl group and sh *ANAX2* group. Tumor volume was measured three times per a week using caliper for 17 days. The tumor incidence was calculated as the ratio of tumor-bearing mice (n) to total mice (n).

Xenograft tumor mouse model carrying shRNA ANXA2 MDA-MB-231 cells to evaluate doxorubicin sensitivity

Balb/c-nude mice (5-weeks old, female) were purchased from ORIENT BIO (Gyeonggi, Korea). The mice were handled using a protocol approved by Duksung Women's University in accordance with the Guidelines for the Care and Use of Laboratory Animals. All animal experiments were carried out in the animal laboratory of Duksung Women's University. Mice were acclimatized for 1 week before the experiment. The sh Ctrl or sh *ANAX2*-transfected MDA-MB-231 cells were orthotopically injected into mammary fat pad with a density of 5×10^6 cells with 100 μl PBS solution containing 10% matrigel ($n = 14$ per group; Corning, 354262). After a week, each mouse transplanted sh Ctrl and sh *ANAX2* cells were divided into four groups randomly ($n = 7$ per group): sh Ctrl-PBS group, sh *ANXA2*-PBS group, sh Ctrl-Doxorubicin group, sh *ANXA2*-Doxorubicin group. Doxorubicin (3 mg/kg, Sigma Aldrich, D1515) was intravenously administered once a week for 33 days. Concurrently, same volume of PBS solute was administered into the sh Ctrl group and sh *ANXA2* group. Tumor size was measured by caliper three times a week for 33 days. At the end of the study, all animals were sacrificed. The excised tumors were obtained and tumor weight was measured. Tumor volumes were calculated by the following formula: Tumor volume (mm^3) = (the length of tumor) × (the width of tumor)^2/2.

Terminal deoxynucleotidyl transferase dUTP nick end labeling (TUNEL) assay

Isolated tumor tissues were gradually frozen with optimal cutting temperature (OCT) compound (Leica Biosystems, 3801480). Frozen tissue blocks were sliced at a thickness of 5 µm using a cryostat (Leica, Nussloch). Cell deaths on tissues were analyzed through TUNEL assay. Briefly, frozen sections were washed with tap water to eliminate OCT compound. After then, the sections were incubated in TdT (Abcam, ab206386) with biotinylated deoxyuridine (Roche Diagnositics, 11093070910) diluted in TdT labeling buffer for 1 h at 37°C in a humidified chamber and washed with termination buffer and distilled water. After washing with terminating buffer and water, the tissues were blocked with 2% BSA in PBS and then washed with PBS. The slices were incubated with avidin-biotin complex (Vector Laboratories, PK-6100), and apoptotic nuclei on tissues were colorized with 3,3-Diaminobenzidine (SK-4100, Vector Laboratories Inc.). Next, the nuclei in the tumor tissues were counterstained with hematoxylin (Merck KGaA, HT40316). Stained tissue sections were observed using microscope (Leica) and quantified by Image J software.

Patient specimens

Nine breast cancer tissues were obtained from patients who underwent mastectomy or breast conserving surgery for breast cancer at Seoul National University Hospital from 2015 to 2016. All patients signed informed consent for the collection of surgical specimens and research analyses (Institutional Review Board no.1405-088-580). Immediately after surgery, the surgeon extracted cancer and normal tissues from the surgical specimen. Blocks of fresh tissue obtained in the operating room were immediately frozen and stored at −70°C.

Analysis of breast cancer database

To analyze the correlation of ANXA2, ATG7, and LC3B expressions, the dataset of human breast tumor tissues from 43 breast cancer patients was downloaded in the GEO database (GSE15852). To analyzed the survival curves following *ANXA2* gene expression, clinical datasets from TNBC patients were downloaded from GEO (GSE36693 and GSE58812). The Kaplan-Meier survival curves for overall survival and metastasis-free survival were constructed and compared by log-rank analysis.

Statistical analysis

Unpaired two-tailed Student's t-test was used to determine significant differences in *in vitro* experiments. A two-way ANOVA followed by Tukey test with repeated measures was used for xenograft tumor models (GraphPad Software, MA). Three independent experiments were performed, and the results were expressed as mean ± S.E.

Disclosure statement

No potential conflict of interest was reported by the author(s).

Funding

The present study was supported by the National Research Foundation of Korea (Nos. 2016R1A6A1A03007648, 2019R1A2C1009773, 2022R1F1A1076029 and 2022R1A2C1093335).

References

[1] Sotiriou C, Neo SY, McShane LM, et al. Breast cancer classification and prognosis based on gene expression profiles from a population-based study. Proc Natl Acad Sci USA. 2003;100(18):10393–10398.
[2] Abramson VG, Mayer IA. Molecular heterogeneity of triple negative breast cancer. Curr Breast Cancer Rep. 2014;6(3):154–158.
[3] Mizushima N. Physiological functions of autophagy. Curr Top Microbiol Immunol. 2009;335:71–84.
[4] Zoncu R, Efeyan A, Sabatini DM. mTOR: from growth signal integration to cancer, diabetes and ageing. Nat Rev Mol Cell Biol. 2011;12(1):21–35.
[5] Zhou H, Huang S. Role of mTOR signaling in tumor cell motility, invasion and metastasis. Curr Protein Pept Sci. 2011;12(1):30–42.
[6] Levy JMM, Towers CG, Thorburn A. Targeting autophagy in cancer. Nat Rev Cancer. 2017;17(9):528–542.
[7] Marsh T, Kenific CM, Suresh D, et al. Autophagic degradation of NBR1 restricts metastatic outgrowth during mammary tumor progression. Dev Cell. 2020;52(5):591–604.
[8] Vera-Ramirez L, Vodnala SK, Nini R, et al. Autophagy promotes the survival of dormant breast cancer cells and metastatic tumour recurrence. Nat Commun. 2018;9(1):1944.
[9] O'Reilly EA, Gubbins L, Sharma S, et al. The fate of chemoresistance in triple negative breast cancer (TNBC). BBA Clin. 2015;3:257–275.
[10] Lefort S, Joffre C, Kieffer Y, et al. Inhibition of autophagy as a new means of improving chemotherapy efficiency in high-LC3B triple-negative breast cancers. Autophagy. 2014;10(12):2122–2142.
[11] Liu C, Sun L, Yang J, et al. FSIP1 regulates autophagy in breast cancer. Proc Natl Acad Sci USA. 2018;115(51):13075–13080.
[12] Wang RX, Xu XE, Huang L, et al. eEF2 kinase mediated autophagy as a potential therapeutic target for paclitaxel-resistant triple-negative breast cancer. Ann Transl Med. 2019;7(23):783.
[13] Wang MC, Wu AG, Huang YZ, et al. Autophagic regulation of cell growth by altered expression of Beclin 1 in triple-negative breast cancer. Int J Clin Exp Med. 2015;8(5):7049–7058.
[14] Choi J, Jung W, Koo JS. Expression of autophagy-related markers beclin-1, light chain 3A, light chain 3B and p62 according to the molecular subtype of breast cancer. Histopathology. 2013;62(2):275–286.
[15] Gerke V, Creutz CE, Moss SE. Annexins: linking Ca2+ signalling to membrane dynamics. Nat Rev Mol Cell Biol. 2005;6(6):449–461.
[16] Wang T, Yuan J, Zhang J, et al. Anxa2 binds to STAT3 and promotes epithelial to mesenchymal transition in breast cancer cells. Oncotarget. 2015;6(31):30975–30992.
[17] Chiang Y, Rizzino A, Sibenaller ZA, et al. Specific down-regulation of Annexin A2 expression in human cells interferes with cell proliferation. Mol Cell Biochem. 1999;199(1–2):139–147.
[18] Sharma MC. Annexin A2 (ANX A2): an emerging biomarker and potential therapeutic target for aggressive cancers. Int J Cancer. 2019;144(9):2074–2081.
[19] Lokman NA, Ween MP, Oehler MK, et al. The role of annexin A2 in tumorigenesis and cancer progression. Cancer Microenviron. 2011;4(2):199–208.
[20] Jeon YR, Kim SY, Lee EJ, et al. Identification of Annexin A2 as a novel secretory biomarker for breast cancer. Proteomics. 2013;13(21):3145–3156.
[21] Sharma MR, Koltowski L, Ownbey RT, et al. Angiogenesis-associated protein Annexin A2 in breast cancer: selective expression in invasive breast cancer and contribution to tumor invasion and progression. Exp Mol Pathol. 2006;81(2):146–156.

[22] Chaudhary P, Gibbs LD, Maji S, et al. Serum exosomal-annexin A2 is associated with African-American triple-negative breast cancer and promotes angiogenesis. Breast Cancer Res. 2020;22(1):11.
[23] Moreau K, Ghislat G, Hochfeld W, et al. Transcriptional regulation of Annexin A2 promotes starvation-induced autophagy. Nat Commun. 2015;6:8045.
[24] Morozova K, Sridhar S, Zolla V, et al. Annexin A2 promotes phagophore assembly by enhancing Atg16L* vesicle biogenesis and homotypic fusion. Nat Commun. 2015;6:5856.
[25] Mukhopadhyay S, Praharaj PP, Naik PP, et al. Identification of Annexin A2 as a key mTOR target to induce roller coaster pattern of autophagy fluctuation in stress. Biochim Biophys Acta Mol Basis Dis. 2020;1866(12):165952.
[26] Dai C, Whitesell L, Rogers AB, et al. Heat shock factor 1 is a powerful multifaceted modifier of carcinogenesis. Cell. 2007;130 (6):1005–1018.
[27] Mendillo ML, Santagata S, Koeva M, et al. HSF1 drives a transcriptional program distinct from heat shock to support highly malignant human cancers. Cell. 2012;150(3):549–562.
[28] Dai C, Sampson SB. HSF1: guardian of proteostasis in cancer. Trends Cell Biol. 2016;26(1):17–28.
[29] Zheng X, Krakowiak J, Patel N, et al. Dynamic control of Hsf1 during heat shock by a chaperone switch and phosphorylation. Elife. 2016;5:e18638.
[30] Desai S, Liu Z, Yao J, et al. Heat shock factor 1 (HSF1) controls chemoresistance and autophagy through transcriptional regulation of autophagy-related protein 7 (ATG7). J Biol Chem. 2013;288(13):9165–9176.
[31] Mizushima N, Yoshimori T, Levine B. Methods in mammalian autophagy research. Cell. 2010;140(3):313–326.
[32] Tanida I, Ueno T, Kominami E. LC3 conjugation system in mammalian autophagy. Int J Biochem Cell Biol. 2004;36 (12):2503–2518.
[33] Collier JJ, Suomi F, Oláhová M, et al. Emerging roles of ATG7 in human health and disease. EMBO Mol Med. 2021;13(12): e14824.
[34] Dunlop EA, Tee AR. mTOR and autophagy: a dynamic relationship governed by nutrients and energy. Semin Cell Dev Biol. 2014;36:121–129.
[35] Feldman ME, Apsel B, Uotila A, et al. Active-site inhibitors of mTOR target rapamycin-resistant outputs of mTORC1 and mTORC2. PLoS Biol. 2009;7(2):e38.
[36] Deora AB, Kreitzer G, Jacovina AT, et al. An annexin 2 phosphorylation switch mediates p11-dependent translocation of annexin 2 to the cell surface. J Biol Chem. 2004;279:43411–43418.
[37] Mosser DD, Morimoto RI. Molecular chaperones and the stress of oncogenesis. Oncogene. 2004;23(16):2907–2918.
[38] Massey AJ, Williamson DS, Browne H, et al. A novel, small molecule inhibitor of Hsc70/Hsp70 potentiates Hsp90 inhibitor induced apoptosis in HCT116 colon carcinoma cells. Cancer Chemother Pharmacol. 2010;66(3):535–545.
[39] Van Durme J, Maurer-Stroh S, Gallardo R, et al. Accurate prediction of DnaK-peptide binding via homology modelling and experimental data. PLoS Comput Biol. 2009;5(8):e1000475.
[40] Lilienbaum A. Relationship between the proteasomal system and autophagy. Int J Biochem Mol Biol. 2013;4(1):1–26.
[41] Seglen PO, Grinde B, Solheim AE. Inhibition of the lysosomal pathway of protein degradation in isolated rat hepatocytes by ammonia, methylamine, chloroquine and leupeptin. Eur J Biochem. 1979;95(2):215–225.
[42] Chen C, Lu L, Yan S, et al. Autophagy and doxorubicin resistance in cancer. Anticancer Drugs. 2018;29(1):1–9.
[43] Gao J, Wang W. Knockdown of galectin-1 facilitated cisplatin sensitivity by inhibiting autophagy in neuroblastoma cells. Chem Biol Interact. 2019;297:50–56.
[44] Chen H, Zhao C, He R, et al. Danthron suppresses autophagy and sensitizes pancreatic cancer cells to doxorubicin. Toxicol in Vitro. 2019;54:345–353.
[45] Zhou Y, Chen E, Tang Y, et al. miR-223 overexpression inhibits doxorubicin-induced autophagy by targeting FOXO3a and reverses chemoresistance in hepatocellular carcinoma cells. Cell Death Dis. 2019;10(11):843.
[46] Cleator S, Heller W, Coombes RC. Triple-negative breast cancer: therapeutic options. Lancet Oncol. 2007;8(3):235–244.
[47] Kaufmann M, Hortobagyi GN, Goldhirsch A, et al. Recommendations from an international expert panel on the use of neoadjuvant (primary) systemic treatment of operable breast cancer: an update. J Clin Oncol. 2006;24 (12):1940–1949.
[48] Faneyte IF, Kristel PM, Maliepaard M, et al. Expression of the breast cancer resistance protein in breast cancer. Clin Cancer Res. 2002;8(4):1068–1074.
[49] Shin HJ, Kwon HK, Lee JH, et al. Doxorubicin-induced necrosis is mediated by poly-(ADP-ribose) polymerase 1 (PARP1) but is independent of p53. Sci Rep. 2015;5:15798.
[50] Xi Y, Ju R, Wang Y. Roles of Annexin A protein family in autophagy regulation and therapy. Biomed Pharmacother. 2020;130:110591.
[51] Gibbs LD, Mansheim K, Maji S, et al. Clinical significance of Annexin A2 expression in breast cancer patients. Cancers (Basel). 2020;13(1):2.
[52] Zhang HT, Zeng Q, Wu B, et al. TRIM21-regulated Annexin A2 plasma membrane trafficking facilitates osteosarcoma cell differentiation through the TFEB-mediated autophagy. Cell Death Dis. 2021;12(1):21.
[53] Wang K, Zhang T, Lei Y, et al. Identification of ANXA2 (annexin A2) as a specific bleomycin target to induce pulmonary fibrosis by impeding TFEB-mediated autophagic flux. Autophagy. 2018;14(2):269–282.
[54] Zhu J, Tian Z, Li Y, et al. ATG7 promotes bladder cancer invasion via autophagy-mediated increased ARHGDIB mRNA stability. Adv Sci (Weinh). 2019;6(8):1801927.
[55] Li M, Liu J, Li S, et al. Autophagy-related 7 modulates tumor progression in triple-negative breast cancer. Lab Invest. 2019;99 (9):1266–1274.
[56] Santagata S, Hu R, Lin NU, et al. High levels of nuclear heat-shock factor 1 (HSF1) are associated with poor prognosis in breast cancer. Proc Natl Acad Sci USA. 2011;108:18378–18383.
[57] Martina JA, Diab HI, Brady OA, et al. TFEB and TFE3 are novel components of the integrated stress response. EMBO J. 2016;35 (5):479–495.
[58] Martina JA, Chen Y, Gucek M, et al. MTORC1 functions as a transcriptional regulator of autophagy by preventing nuclear transport of TFEB. Autophagy. 2012;8(6):903–914.
[59] Kim S, Song G, Lee T, et al. PARsylated transcription factor EB (TFEB) regulates the expression of a subset of Wnt target genes by forming a complex with β-catenin-TCF/LEF1. Cell Death Differ. 2021;28(9):2555–2570.
[60] Arias E, Koga H, Diaz A, et al. Lysosomal mTORC2/PHLPP1/Akt regulate chaperone-mediated autophagy. Mol Cell. 2015;59(2):270–284.
[61] Renna M, Bento CF, Fleming A, et al. IGF-1 receptor antagonism inhibits autophagy. Hum Mol Genet. 2013;22(22):4528–4544.
[62] Holmes B, Benavides-Serrato A, Freeman RS, et al. mTORC2/AKT/HSF1/HuR constitute a feed-forward loop regulating rictor expression and tumor growth in glioblastoma. Oncogene. 2018;37 (6):732–743.
[63] Lei H, Romeo G, Kazlauskas A. Heat shock protein 90alpha-dependent translocation of Annexin A2 to the surface of endothelial cells modulates plasmin activity in the diabetic rat aorta. Circ Res. 2004;94(7):902–909.
[64] Kang R, Zeh HJ, Lotze MT, et al. The Beclin 1 network regulates autophagy and apoptosis. Cell Death Differ. 2011;18(4):571–580.
[65] Chang Z, Shi G, Jin J, et al. Dual PI3K/mTOR inhibitor NVP-BEZ235-induced apoptosis of hepatocellular carcinoma cell lines is enhanced by inhibitors of autophagy. Int J Mol Med. 2013;31(6):1449–1456.
[66] Jain K, Paranandi KS, Sridharan S, et al. Autophagy in breast cancer and its implications for therapy. Am J Cancer Res. 2013;3(3):251–265.
[67] Koh M, Woo Y, Valiathan RR, et al. Discoidin domain receptor 1 is a novel transcriptional target of ZEB1 in breast epithelial cells undergoing H-Ras-induced epithelial to mesenchymal transition. Int J Cancer. 2015;136(6):E508–520.